

## Performance evaluation of aqueous all iron redox flow batteries using heat treated graphite felt electrode

Hyeonsoo Lim<sup>\*,‡</sup>, Mingyu Shin<sup>\*,‡</sup>, Chanho Noh<sup>\*\*</sup>, Eeungmo Koo<sup>\*\*</sup>,  
Yongchai Kwon<sup>\*,\*\*,\*†</sup>, and Kun Yong Chung<sup>\*,\*\*,\*†</sup>

<sup>\*</sup>Department of New and Renewable Energy Convergence, Seoul National University of Science and Technology,  
232, Gongneung-ro, Nowon-gu, Seoul 01811, Korea

<sup>\*\*</sup>Department of Chemical and Energy Engineering, Seoul National University of Science and Technology,  
232, Gongneung-ro, Nowon-gu, Seoul 01811, Korea

(Received 5 April 2022 • Revised 16 May 2022 • Accepted 2 June 2022)

**Abstract**—The effect of heat treatment of graphite felt (GF) electrode on the performance of aqueous redox flow batteries (ARFBs) using Ferrocyanide and iron-3-[Bis(2-hydroxyethyl)amino]-2-hydroxy-propanesulfonic acid complex (Fe(DIPSO)) as redox couple was evaluated. For the heat treatment of GF, temperature and retention time were determined as main parameters to affect the performance of ARFB. With their changes, the double layer capacitance (DLC) and surface area of GF electrodes were varied. When GF was heat treated at 600 °C for 1 h, its DLC and surface area were best as 0.3708 F g<sup>-1</sup> and 1.8408 m<sup>2</sup> g<sup>-1</sup>. With the enhancements in DLC and surface area, the redox reactivity of Ferrocyanide and Fe(DIPSO) also improved, while their charge transfer resistance reduced. When the heat treated GF was used as electrodes, ARFB single cell using Ferrocyanide and Fe(DIPSO) showed better performance than ARFB single cell using pristine GF without heat treatment. For example, with the heat-treated GF, energy efficiency increased from 56 to 63% at a high current density of 200 mA cm<sup>-2</sup>, and its maximum power density was 14% more improved.

Keywords: Redox Flow Battery, Graphite Felt, Heat Treatment, Hydrophilicity, All-iron Battery

### INTRODUCTION

Energy production continuously increases due to the increasing global energy demand. Among the various energy production methods, power generation using fossil fuels induces serious environmental pollution problems, followed by global warming. Renewable energies were proposed as an alternative to solve these problems [1,2]. As the representative renewable energy sources, there are solar and wind power energies. When these renewable energies are produced, the emission of environmental pollutants such as sulfur oxides and nitrogen oxides is alleviated, while the emission of carbon dioxide is also suppressed [3]. Therefore, the development of renewable energies to replace the fossil fuel based classical energies significantly is required [4]. In spite of that, such renewable energies have severe limitations due to their typical drawbacks of intermittent and unstable power generation [5,6]. Therefore, both storing the power produced by renewable energy sources with peak shaving or load leveling and supplying the power to the power grid are important, and energy storage systems (ESSs) can play a role [7-9].

Among the various ESSs, ESSs using secondary battery are denoted as battery ESSs (BESSs) and lithium-ion batteries (LIBs) are famous as such BESSs [10]. However, since LIBs are weak to fire and explosion when they are prepared for large scale applica-

tions, developing new battery systems that can overcome the roadblocks of the conventional LIBs is needed [11]. One promising candidate is the redox flow battery (RFB). The RFBs consist of cells where the actual electrochemical reactions occur, electrolyte tanks storing electrolytes, and pumps circulating the electrolytes. Here, the redox active materials are dissolved in supporting electrolytes, and they are stored in electrolyte tanks [12,13]. Electrolytes including redox active materials and supporting electrolytes are circulated to RFB cell through pumps, and undergo electrochemical reactions at electrodes, and they are again stored in the electrolyte tanks [14, 15]. Electrodes of RFB cell do not directly participate in electrochemical reactions, but only provide active sites for the reactions. Due to the routine, the damages of electrodes are minimized, while the possibility of degradation of electrolytes is lowered, resulting in a longer lifespan of RFBs than other batteries [16]. In addition, since RFBs have excellent design flexibility controlling their power and capacity separately, they are very appropriate to be used for ESSs [17-20].

So far, the most studied RFB is all-vanadium RFB (VRFB), which uses vanadium ions as active materials for both electrolytes that are denoted as posolyte and negolyte, while its theoretical cell voltage is 1.26 V [21-23]. Although this VRFB has several advantages and has been actively studied to date, there are unique problems such as expensive cost and narrow operable temperature ranges. Therefore, various studies to replace the vanadium active material are ongoing [12,24-26]. For example, organic materials such as anthraquinone, benzoquinone, quinoxaline, and metals such as Ni and Fe are the candidates [27-31].

<sup>†</sup>To whom correspondence should be addressed.

E-mail: kwony@seoultech.ac.kr, kychung@seoultech.ac.kr

<sup>‡</sup>H. Lim and M. Shin contributed equally to this work.

Copyright by The Korean Institute of Chemical Engineers.

As one of them, metalorganic materials are also promising. They consist of transition metals and organic ligands, and so far, iron-1,3-diaminopropanetetraacetic acid complex (Fe(PDTA)), iron-diethylenetriaminepentaacetic acid complex (Fe(DTPA)), iron-3-[Bis(2-hydroxyethyl)amino]-2-hydroxy-propanesulfonic acid complex (Fe(DIPSO)), cobalt-triisopropanolamine complex (Co(TIPA)) and cobalt-triethanolamine complex (Co(TEA)) have been used [32-34]. They have the strong benefits such as easy control of redox potential, cheap cost, and low crossover [35,36]. In previous studies, when ARFB using Ferrocyanide and Fe(DIPSO) as redox couple was operated, the theoretical open circuit voltage (OCV) was 1.37 V, while they were stably operated for more than 100 cycles with energy efficiency (EE) of 70% at 80 mA cm<sup>-2</sup> [37].

Besides discovering new active materials, using catalyst or modified electrode is another way to improve the performance of RFB [38,39]. Especially, the heat treatment of electrode can be beneficial because this is a relatively simple and economic way to enhance the quality of electrode [40]. As the electrode for RFBs, graphite felts (GFs) have been mainly used. When GFs are heat treated, it is expected that their active surface area and the portion of oxygen functional groups will increase. As a result, charge transfer promoted by the redox reactions of active materials will be further facilitated and eventually, the performance of RFB will increase [41,42].

To date, there have been many studies that reported improvements in performance of RFBs through the heat treatment of carbon-based electrodes. For instance, Jing et al. did heat treatment of carbon felt for VRFB under CO<sub>2</sub> condition [43]. Due to the heat treatment, energy efficiency (EE) of VRFB was improved from 79.28 to 84.1%. Chang et al. used CO<sub>2</sub>-activated carbon felt for VRFB [44]. By the activation process of carbon felt electrode, EE of VRFB was 18% more improved than that of VRFB using pristine carbon electrode. Dong et al. used the heat-treated carbon paper electrodes in RFBs using Ti and Mn as redox couple [45]. Mazúr group confirmed the performance improvement in VRFBs through heat treatment of graphite felt [42]. Taken together, when heat treatment process is performed under CO<sub>2</sub> condition, a high temperature range of 900-1,000 °C is required. On the other hand, when the heat treatment process is carried out under air, the needed temperature range is 400-700 °C. This means that when ambient air is utilized for heat treatment, this treatment will be simpler and more economical than using CO<sub>2</sub> condition.

However, there were few results studying the effects of the treatments of electrode on the redox reactivity of metalorganic active materials considered in RFBs and the performance of the RFBs. Therefore, it is appropriate to investigate whether the heat treatment of electrodes can affect the redox reactivity of metalorganic active materials and the performance of RFBs using them.

Based on that, in this study, the effect of the heat treatment of GF electrodes on the performance of RFBs using metalorganic active materials was evaluated. Here, as the metalorganic active materials, Ferrocyanide and Fe(DIPSO) were determined. For the heat treatment of GF electrodes, temperature and retention time were mainly controlled, and the structural properties of the heat-treated GF electrodes were investigated by measuring double layer capacitance (DLC) and Brunauer-Emmett-Teller (BET) specific surface area, while their electrochemical properties were estimated by using

cyclic voltammetry (CV). In turn, the performance of RFB single cells using the heat-treated GF electrodes was measured.

## EXPERIMENTAL

### 1. Graphite Felt Heat Treatment

For tests, graphite felt (GFD 4.6, Sigracell) was used. The heat treatment was at various temperatures (200, 300, 400, 500, 600, and 700 °C) in ambient static air atmosphere using a furnace (JSMF-30T, JSR, Korea). Then, heat treatments were carried out at various times (30 min, 1 h, 2 h, 3 h, 4 h, and 5 h) under 600 °C because when heat treatment temperature was 600 °C, its effect on the properties of GFs was best. The temperature ramping rate was 10 °C min<sup>-1</sup>.

### 2. Electrode Characterization

To confirm the overall thermal stability of graphite felt and the proper temperature for heat treatment, thermogravimetric analysis (TGA, SDT Q 600) was used. To measure the physical surface area of GF electrodes after heat treatment, a multiport chemisorption/physisorption/micropore analyzer (3flex, Micromeritics, USA) was used. Changes in the surface morphology of the GF electrodes were examined by using scanning electronic microscopy (SEM, JSM-7610F, JEOL). X-ray photoelectron spectroscopy (XPS, K-Alpha+, Thermo Scientific) was used to evaluate their surface components and changes before and after the heat treatment. When C1s spectra of the GF electrodes were analyzed, the main peaks for C-C (SP2), C-C (SP3), C-O, and C=O were observed at 284.15, 284.95, 286, and 287.25 eV, respectively. In addition, the main peaks for O=C, O-C, and H-O-H of O1s were observed at 530.9, 532.425, and 534.95 eV. For the XPS characterization, samples were mounted onto the container made up by copper conductive tape, and the container was transferred to the chamber of XPS. XPS analysis was carried out with pass energy of 200.0 eV and energy step size of 1.0 eV. On the same spot, spectra of O1s and C1s were collected with pass energy of 50.0 eV and energy step size of 0.10 eV and were deconvoluted to recognize the chemical bonds doped on the surface of the GF electrode samples.

### 3. Electrochemical Characterization

Three-electrode half-cell was used for electrochemical evaluation. As a working electrode, GFs with diameter of 1 cm were used, while Pt wire and silver chloride electrode (Ag/AgCl) were used as counter and reference electrodes. The solutions used in these experiments were prepared using a method previously reported [37]. To synthesize Fe(DIPSO) as negolyte, 2.665 g of Fe<sub>2</sub>(SO<sub>4</sub>)<sub>3</sub> was dissolved into 10 mL of deionized water (DIW) and the solution was stirred for 10 min. Then, 3.6859 g of DIPSO was added to the solution and stirred for 10 min. Next, 4.8267 g of KOH was added with stirring for 24 h. The volume of the mixture solution was adjusted to 20 mL. Finally, precipitated K<sub>2</sub>SO<sub>4</sub> that was contained in the solution was separated by using a centrifuge. To prepare for Ferrocyanide solution as negolyte, Ferrocyanide was dissolved into 10 mL of DIW and the solution was stirred for 10 min. After stirring, KOH was added into the solution with stirring for 24 h. The volume of the mixture solution was also adjusted to 20 mL.

Cyclic voltammetry (CV) was used to measure the DLC of each GF and the reactivity between active material and GF. For mea-

measuring DLC, 1 M KOH solution was used as supporting electrolyte, and the applied potential range for CV curve measurements was from  $-0.15$  to  $0.03$  V (vs. Ag/AgCl). The measurements were conducted at various scan rates ( $5, 10, 20$ , and  $30$  mV s $^{-1}$ ). After that, DLC was calculated using Eq. (1). In Eq. (1),  $Q$ ,  $E$ ,  $i$ , and  $t$  mean charge, potential, current, and time, respectively [46].

$$\text{DLC} = \frac{\Delta Q}{\Delta E} = \frac{\int_{E_1}^{E_2} i \, dt}{E_2 - E_1} \quad (1)$$

For measuring the CV curves evaluating the reactivity of active material and GFs, active material concentration of  $0.01$  M was determined, and 1 M KOH solution was used as a supporting electrolyte. The voltage scan range for Fe(DIPSO) solution was  $-1.3$ ~ $-0.3$  V (vs. Ag/AgCl) and that for Ferrocyanide solution was  $0$ ~ $0.55$  V (vs. Ag/AgCl). The peak separation and peak current density are measured in CV curve measurements.

In electrochemical impedance spectroscopy (EIS), posolyte and negolyte conditions were the same as those of the solution conducted in the CV test. The cathode test was conducted at  $-1.00$  V (vs. Ag/AgCl), and the frequency range was  $0.1$  Hz to  $100$  KHz. The anode test was conducted at  $0.18$  V (vs. Ag/AgCl), and the frequency range was  $0.1$  Hz to  $100$  KHz [47,48].

RFB single cell tests were conducted to evaluate their performance. For the tests, the area of GF electrode was  $2 \times 2$  cm $^2$ , while Nafion 212 (Chemours, USA) was used as ion exchange membrane. The membrane was immersed in DIW for 24 h before the test. Electrolyte including  $0.5$  M Sodium Ferrocyanide,  $0.3$  M Potassium Ferricyanide, and  $1$  M Potassium hydroxide ( $20$  mL) was considered as posolyte, while that including  $0.5$  M Fe(DIPSO) and  $4$  M Potassium hydroxide ( $19$  mL) was negolyte. For RFB step test, five cycles were performed at  $80, 120, 160$ , and  $200$  mA cm $^{-2}$ , respectively, and then the current density was recovered to  $80$  mA cm $^{-2}$ , and 15 cycles were further performed. At this time, cut-off voltage range was  $0.75$  to  $1.75$  V. For a long cycle test, 100 cycles of RFB single cells were run at  $200$  mA cm $^{-2}$ .

## RESULT AND DISCUSSION

### 1. Optimal Conditions for the Heat Treatment of GFs

The heat treatment of GF samples is one of basic methods. To determine its suitable condition, heating temperature was initially handled, and heating time was then optimized. First, the heat treatment of GF samples was performed for 1 h at each temperature, while DLC of such heat-treated GF samples was measured to evaluate the actual impact of heat treatment. As the heating tempera-

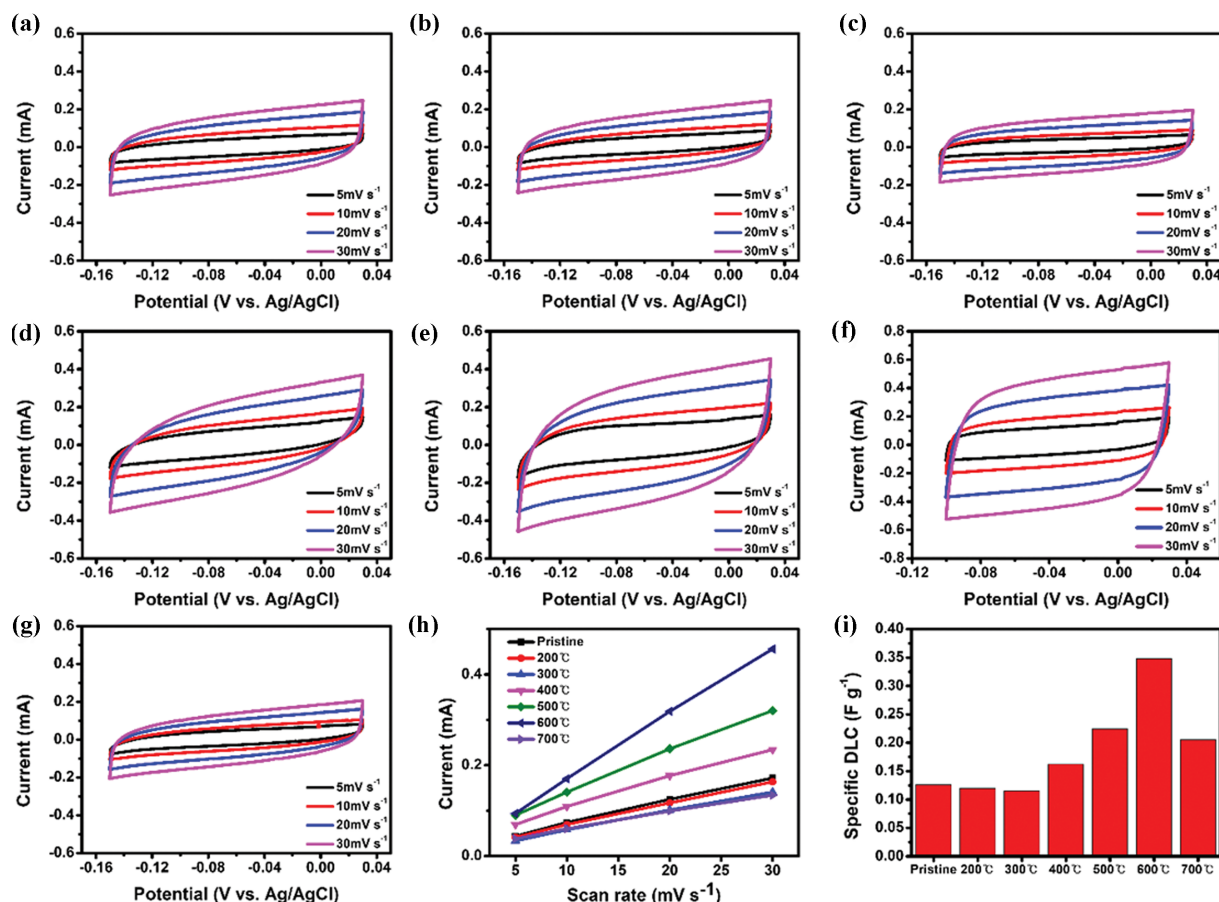


Fig. 1. Cyclic voltammograms of (a) pristine felt, (b) 200 °C, (c) 300 °C, (d) 400 °C, (e) 500 °C, (f) 600 °C and (g) 700 °C 1 h treated felt in various scan rate; (h) anodic currents of the recorded CVs at  $-0.04$  V (vs. Ag/AgCl) vs. scan rate; (i) the corresponding specific double layer capacitance of treated felts.

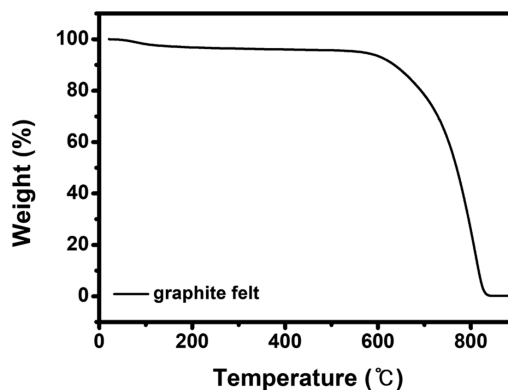
**Table 1.** The average weight change of felts before and after thermal treatments

Processing time: 1 h	200 °C	300 °C	400 °C	500 °C	600 °C	700 °C
Weight change	−0.13%	−0.05%	−0.11%	−0.56%	−3.25%	−43.65 %

ture, from 200 to 700 °C was set with an interval of 100 °C (Fig. 1). As shown in Fig. 1, pristine GF showed DLC of 0.1259 F g<sup>−1</sup>, and that of GF treated at 600 °C was 0.3708 F g<sup>−1</sup>, while the DLC rapidly decreased when the heat treatment temperature reached 700 °C. The improvement in DLC was related to the physical surface area that increased by impeding damage to the GF fiber surfaces through heat treatment in air condition. When the heat temperature was higher than 700 °C, the GF was seriously damaged (Table 1, Fig. 2). TGA also showed rapid weight reduction at a higher temperature than 600 °C. This means that 600 °C is a suitable temperature for the heat treatment of GF.

Based on the above results, the heat treatment temperature was determined as 600 °C.

After determining the heat treatment temperature as 600 °C, the proper heating time was decided. DLC of GF samples measured in each heating time is represented in Fig. 3. According to Fig. 3, when the heat treatment was at 600 °C, DLC increased when the time reached 1 h, and after that, DLC decreased. Quantitatively, DLC

**Fig. 2.** Thermogravimetric analysis of graphite felt.

increased from 0.1259 to 0.3708 F g<sup>−1</sup> for 1 h treatment and then decreased to 0.2653 and 0.2029 F g<sup>−1</sup> at 2 h and 3 h treatment, respectively. When the weight of GF samples before and after heat

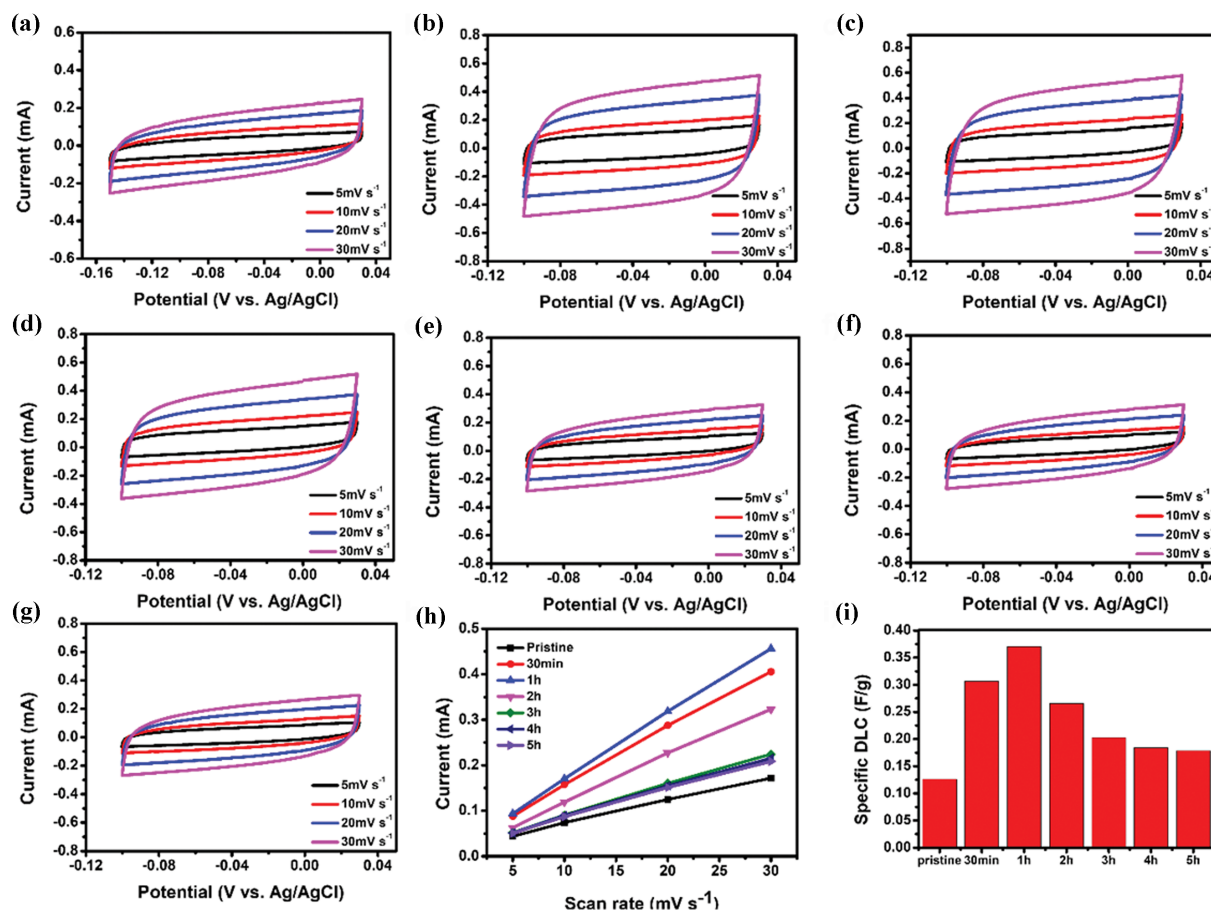


**Fig. 3.** Cyclic voltammograms of (a) pristine felt, (b) 30 min, (c) 1 h, (d) 2 h, (e) 3 h, (f) 4 h and (g) 5 h treated felt at 600 °C in various scan rate; (h) anodic currents of the recorded CVs at −0.04 V (vs. Ag/AgCl) vs. scan rate; (i) the corresponding specific double layer capacitance of treated felts.

treatment was compared, an average weight loss of 4.0% was recorded at 1 h treatment, while at 3 h treatment, the weight loss was 8.7% (Table 2). This supports the fact that the properties of GF

samples are degraded by the heat treatment more than 1 h. With that, it is confirmed that the properties of GF samples are optimized when heat treatment is performed for 1 h at 600 °C.

**Table 2.** The average weight change of felts before and after thermal treatments

Processing temperature: 600 °C	30 min	1 h	2 h	3 h	4 h	5 h
Weight change	−2.01%	−3.98%	−6.39%	−8.72%	−12.48%	−15.08%

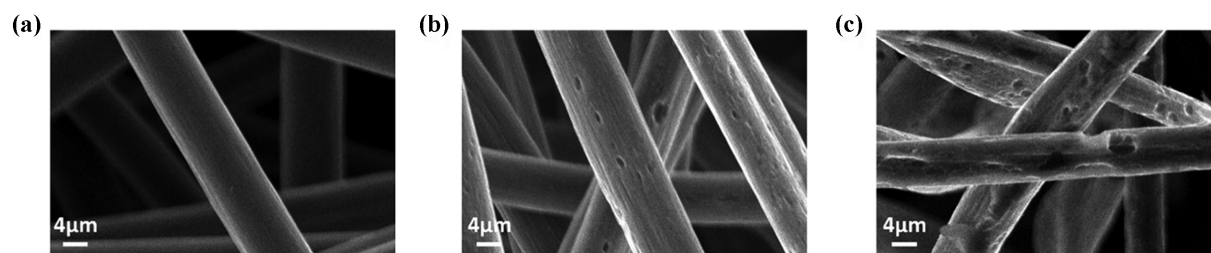


**Fig. 4.** The SEM image of (a) pristine felt, (b) 600 °C+1 h heat treated GF and (c) 600 °C+3 h heat treated GF.

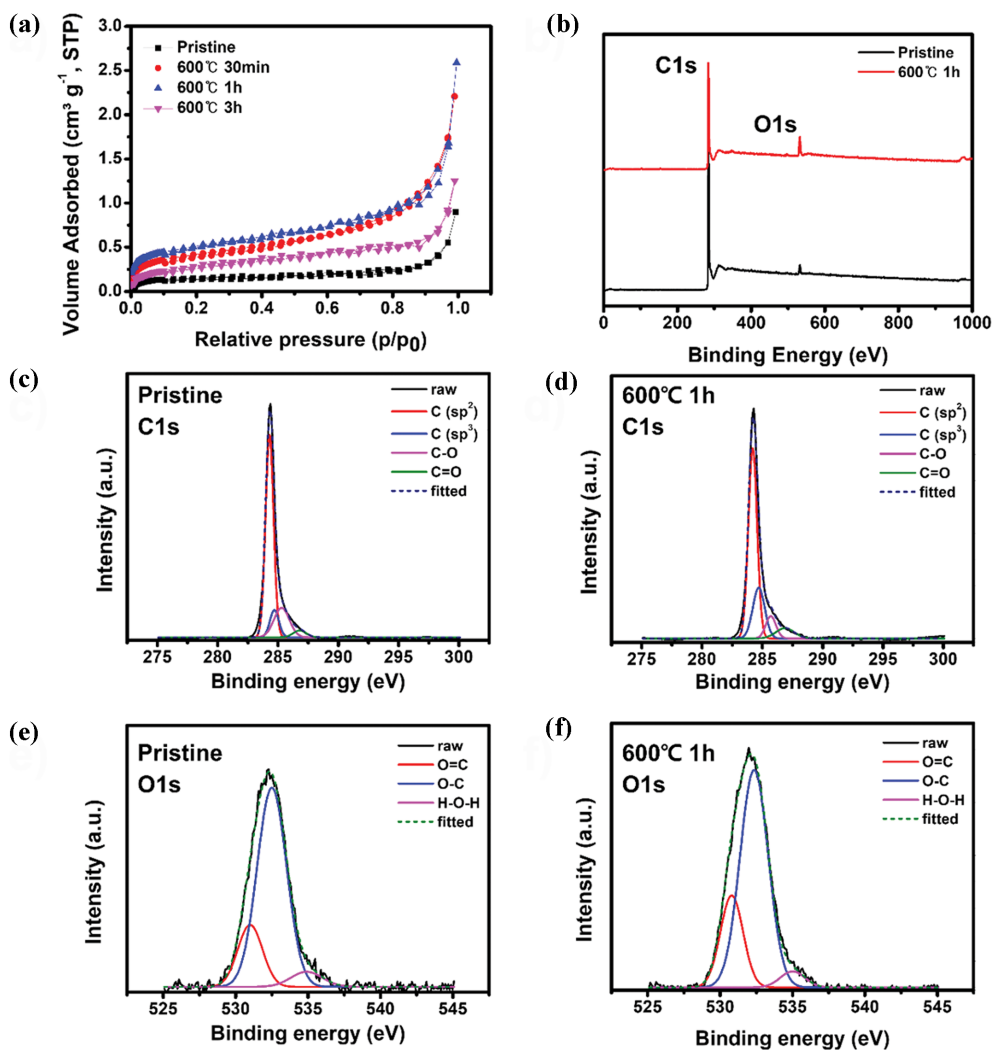


**Fig. 5.** (a) BET adsorption and desorption graphs of pristine and treated felts; (b) The XPS spectra of pristine felt and 600 °C/1-hour heat treated felt; Spectra for C 1s of (c) pristine felt, (d) 600 °C/1-hour heat treated felt and spectra for O 1s of (e) pristine felt, (f) 600 °C/1-hour heat treated felt.



To inspect optically the heat treatment of GF, the surface of the heat-treated GF samples was measured by SEM (Fig. 4). In Fig. 4, the fiber surfaces of GF were smooth before heat treatment, while pores were formed on the GF fiber surface after heat treatment. With that, it is substantiated that surface area of GF greatly increases when pores are generated [42,49]. Furthermore, due to the formation of pores, it is expected that the mass transfer of active materials will be facilitated [49,50]. In Fig. 4(c), the surface of 600 °C+3 h heat treated GF sample was more significantly damaged than that of 600 °C+1 h heat treated GF sample. This also well agreed with the previous experimental results (Table 2 and Fig. 3).

The physical surface area of GF sample was then quantitatively evaluated through BET measurements (Fig. 5). In Fig. 5, the surface area of each GF sample increased to 0.5959, 1.5146, and 1.8408 m<sup>2</sup> g<sup>-1</sup> at pristine felt, 30 min, and 1 h treated GF samples, respectively, while this decreased to 1.0284 m<sup>2</sup> g<sup>-1</sup> after 3 h heat treatment. This was a similar trend to DLC measurements.

To further investigate the surface of GF samples, XPS analysis was implemented (Fig. 5). According to Fig. 5, the portion of oxygen functional groups in the surface of GF samples increased after heat treatment (Fig. 5(b)-(f)). Quantitatively, in pristine GF, the portion was 3.04 atomic%, while the portion increased to 9.46 atomic% in 600 °C+1 h heat treated GF. This indicates that the oxygen functional groups were generated on the surface of GF by the heat treatment. It is then expected that the hydrophilicity of the GF electrode will increase because the oxygen functional groups promote the hydrophilicity of surface, while such enhanced hydrophilicity will improve the redox reactivity of active materials that

occurs on the surface of GF electrode. Based on these evaluations, the best heat treatment condition of GF electrode was determined as 600 °C and 1 h. For the sequential tests, the GFs using this condition were denoted as heat-treated felts.

## 2. Electrochemical Reactivity and RFB Single Cell Performance Evaluation

Based on the previous results, electrochemical evaluations were further performed to investigate whether the heat treated GF electrode can affect the redox reactivity of active materials (Fig. 6).

According to Figs. 5(a) and (b), the redox reactivity of both Fe(DIPSO) and Ferrocyanide was increased by the use of the heat treated GF electrode. More specifically, the peak current density of Fe(DIPSO) and Ferrocyanide was improved by 7.6 and 18.7% compared to that when using pristine GF electrode. In addition, 600 °C+3 h heat treated GF sample showed a lower reactivity than 600 °C+1 h heat treated GF sample, which indicates a similar trend to the measurements of DLC and surface area.

Figs. 6(c) and 6(d) represent Nyquist plot of each heat treated GF sample. When compared with the pristine GF sample, charge transfer resistance ( $R_{ct}$ ) of 600 °C+1 h heat treated GF samples was decreased from 2.3 to 1.4 Ω in Fe(DIPSO) solution, while this was also decreased from 2.7 to 1.9 Ω in Ferrocyanide solution. In addition,  $R_{ct}$  of 600 °C+3 h heat treated GF samples was larger than that of 600 °C+1 h heat treated GF samples. In Fe(DIPSO),  $R_{ct}$  of 600 °C+3 h heat treated GF samples was 1.7 Ω, while this was 2.3 Ω in Ferrocyanide. This implies that  $R_{ct}$  is smallest in 600 °C+1 h heat treated GF samples, and this trend is consistent with the previous results. Such improvements in redox reactivity and  $R_{ct}$  are probably attributed

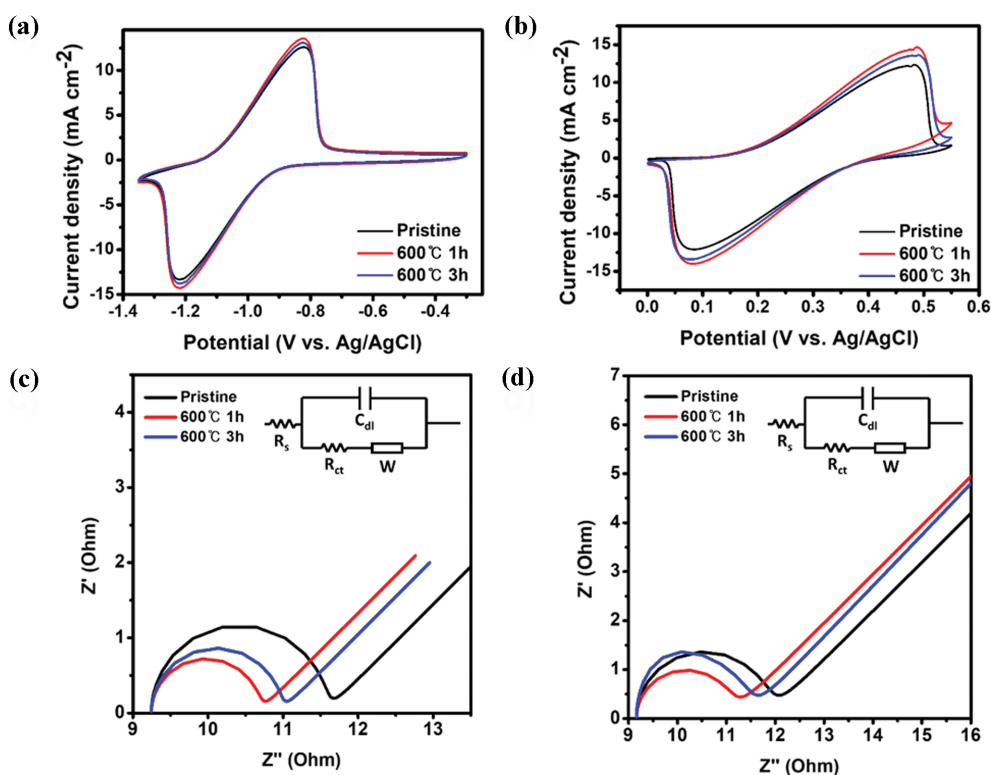


Fig. 6. Cyclic voltammograms of (a) Fe(DIPSO) and (b) Ferrocyanide solution using pristine and heat-treated GF electrode; electrochemical impedance spectroscopy graphs of (c) Fe(DIPSO) and (d) Ferrocyanide solution using pristine and heat-treated GF electrode.

tional groups of GF electrode.

As the next step, the effects of the heat treated GF electrodes on the performances of RFBs using Fe(DIPSO) and Ferrocyanide as redox couple were investigated. For that, cycle tests of such RFB single cells were conducted (Fig. 7). Here, pristine GF and 600 °C+3 h heat treated GF electrodes were used as control groups. In Fig. 7(a), when the same cut-off voltage range was set, as current density increased, charging/discharging capacity decreased by the increased overpotential. More specifically, the pristine GF electrode showed a capacity retention rate of 73.3% at 200 mA cm<sup>-2</sup>, whereas that of 600 °C+1 h heat treated GF electrode was 86.9%. As shown in Fig. 7(c), coulombic efficiency (CE) of RFB single cells was well maintained as 99.9% in all electrodes, which means that other side reactions do not occur over the cycling tests of RFB single cells,

while the performance degradation of RFB single cells occurs due to the decrease in energy efficiency (EE) by the increase in current density.

Regarding EE of RFB single cells as shown in Fig. 7(b), that of RFB single cells using heat-treated GF electrodes was better than that using pristine GF electrode in all current densities that correspond to 200 mA cm<sup>-2</sup>. Quantitatively, EE of RFB single cell using pristine GF electrode was 56.1%, while that using 600 °C+1 h heat treated GF electrode was 62.9%. According to Fig. 7(d), the over-voltage was reduced when the 600 °C+1 h heat treated GF electrode was used. In summary, the performance of RFB single cells using Fe(DIPSO) and Ferrocyanide as redox couple was best when the 600 °C+1 h heat treated GF electrode was used.

Next, the long-term stability of RFB single cell using 600 °C+1 h

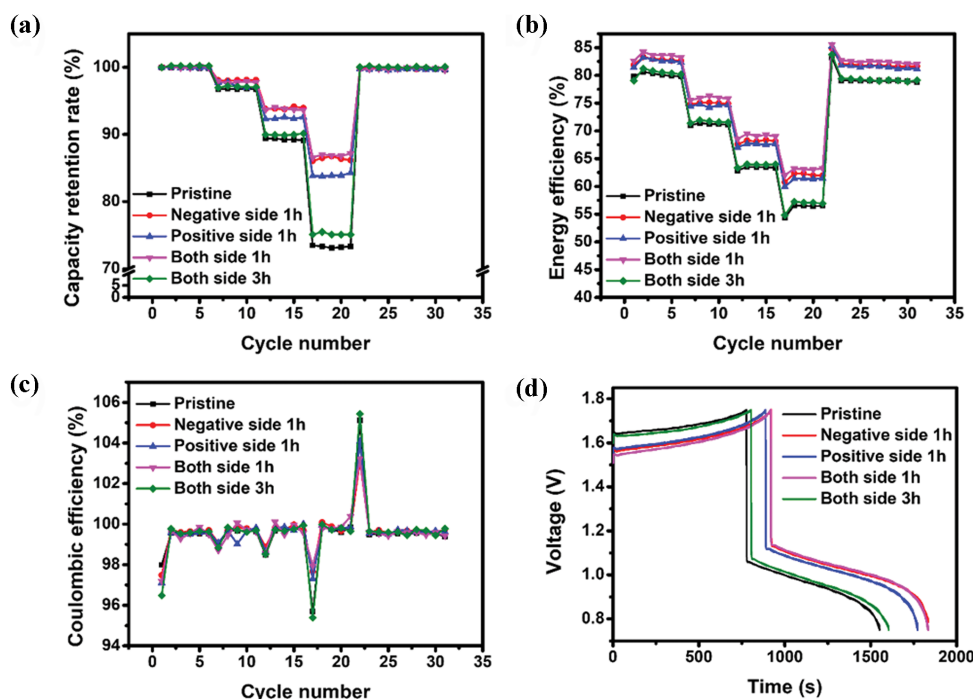


Fig. 7. (a) Capacity retention rates, (b) Energy efficiency, (c) Coulombic efficiency measured at various current densities of 80 mA cm<sup>-2</sup> (1-6 cycles), 120 mA cm<sup>-2</sup> (7-11 cycles), 160 mA cm<sup>-2</sup> (12-16 cycles), 200 mA cm<sup>-2</sup> (17-21 cycles) and 80 mA cm<sup>-2</sup> (22-31 cycles) and (d) charge/discharge graphs of Fe(DIPSO)/Ferrocyanide RFB single cell with various felts.

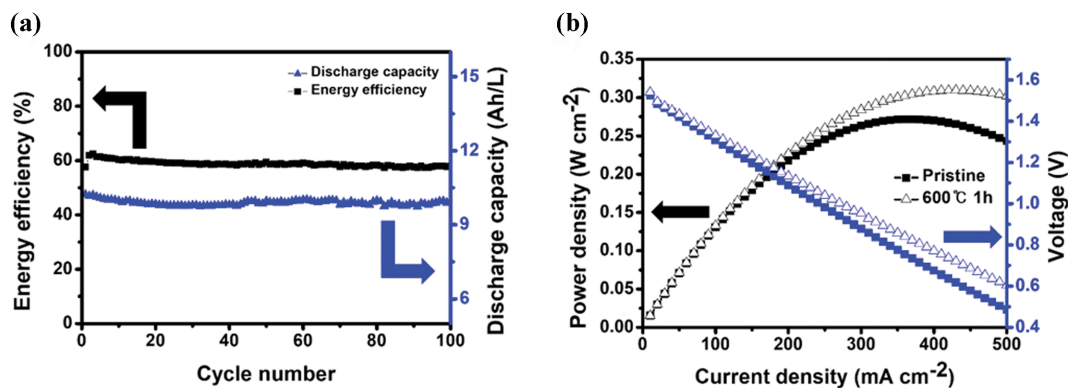


Fig. 8. (a) Energy efficiency, discharge capacity of Fe(DIPSO)/Ferrocyanide RFB single cell using 600 °C+1 h heat treated GF and (b) the polarization curve of Fe(DIPSO)/Ferrocyanide RFB single cell using pristine felt and 600 °C+1 h heat treated GF.

heat treated GF electrode was evaluated (Fig. 8). For doing that, such an RFB single cell was operated for 100 cycles at  $200 \text{ mA cm}^{-2}$ . As a result, as shown in Fig. 8(a), the RFB single cell using  $600^\circ\text{C}+1 \text{ h}$  heat treated GF electrode showed an average capacity of  $9.9 \text{ Ah L}^{-1}$  and EE of 58.8% for 100 cycles. This means that even in a long cycle test, RFB single cell using  $600^\circ\text{C}+1 \text{ h}$  heat treated GF electrode preserved its performance well. In spite of that, due to the stability issue of electrolyte including Ferrocyanide revealed in previous study, a little degradation of efficiency was observed as time elapsed, while this issue should be solved soon [37]. In Fig. 8(b), maximum power density (MPD) of RFB single cells using pristine GF and  $600^\circ\text{C}+1 \text{ h}$  heat treated GF electrodes was recorded. When pristine GF electrode was used, MPD of RFB single cell was  $0.272 \text{ W cm}^{-2}$  at  $370 \text{ mA cm}^{-2}$ , while that of RFB single cell using  $600^\circ\text{C}+1 \text{ h}$  heat treated GF electrode was improved as  $0.310 \text{ W cm}^{-2}$  at  $430 \text{ mA cm}^{-2}$ . This confirms that RFB single cell using  $600^\circ\text{C}+1 \text{ h}$  heat treated GF electrode induces high MPD.

## CONCLUSION

This study confirmed performance improvement in RFB using a Fe(DIPSO)/Ferrocyanide redox couple through heat treatment of GF. Heat treatment in air conditions etched the surface of the felt, thereby increasing the surface area. In addition, the hydrophilicity was increased due to the increase of the oxygen functional group, and the reactivity with the electrolyte was increased, thereby improving the performance. However, if it is treated at too high a temperature or for a long time, the damage to the felt increases and the performance decreases. Therefore, the appropriate treatment temperature and time were optimized. For optimization, the condition with the largest electrical surface area was found through DLC measurement, and the physical surface area was also confirmed through BET. The same trend can be seen with the DLC and BET results from the SEM images. These treatments and analyses confirmed the optimal treatment condition for the DLC, and the physical surface area was improved to  $0.3708 \text{ F g}^{-1}$  and  $1.8408 \text{ m}^2 \text{ g}^{-1}$ , respectively, at  $600^\circ\text{C}$  for 1 h. Next, single cell tests were conducted to confirm whether this result was effective in the actual RFB system. As a result of single cell tests, the energy efficiency was improved from 56.1% to 62.9% at  $200 \text{ mA cm}^{-2}$ , and this trend was maintained even in the experiment for 100 cycles. In addition, 13.97% higher MPD can be obtained from RFB using treated felt than that using pristine through MPD measurement. Through this study, it can be confirmed that the performance improvement method through electrode treatment used in other RFBs is also useful in the Fe(DIPSO)/Ferrocyanide RFB of previous studies. Therefore, it is expected that performance improvement of all-iron aqueous RFB using Fe(DIPSO)/Ferrocyanide redox couple can be obtained by using various methods for improving the felt surface area studied in the existing VRFB. Moreover, it is possible to manufacture electrodes for all-iron RFB using the existing felt manufacturing process.

## ACKNOWLEDGEMENT

This study was supported by the Research Program funded by the

SeoulTech (Seoul National University of Science and Technology).

## REFERENCES

1. Z. Yang, J. Zhang, M. C. W. Kintner-Meyer, X. Lu, D. Choi, J. P. Lemmon and J. Liu, *Chem. Rev.*, **111**, 3577 (2011).
2. C. Noh, M. Jung, D. Henkensmeier, S. W. Nam and Y. Kwon, *ACS Appl. Mater. Interfaces*, **9**, 36799 (2017).
3. F. A. Rahman, M. M. A. Aziz, R. Saidur, W. A. W. A. Bakar, M. R. Hainin, R. Putrajaya and N. A. Hassan, *Renew. Sustain. Energy Rev.*, **71**, 112 (2017).
4. M. Jung, W. Lee, N. Nambi Krishnan, S. Kim, G. Gupta, L. Komsiyyska, C. Harms, Y. Kwon and D. Henkensmeier, *Appl. Surf. Sci.*, **450**, 301 (2018).
5. S. R. Bull, *Proc. IEEE*, **89**, 1216 (2001).
6. B. Hayman, J. Wedel-Heinen and P. Brøndsted, *MRS Bull.*, **33**, 343 (2008).
7. H. Chen, T. N. Cong, W. Yang, C. Tan, Y. Li and Y. Ding, *Prog. Nat. Sci.*, **19**, 291 (2009).
8. S. Moon, B. W. Kwon, Y. Chung and Y. Kwon, *J. Electrochem. Soc.*, **166**, A2602 (2019).
9. W. Lee, G. Park, D. Schröder and Y. Kwon, *Korean J. Chem. Eng.*, **38**, 1 (2022).
10. K. Smith, A. Saxon, M. Keyser, B. Lundstrom, Z. Cao and A. Roc, in *2017 Am. Control Conf.*, 4062 (2017).
11. L. Kong, C. Li, J. Jiang and M. G. Pecht, *Energies*, **11**, 1 (2018).
12. W. Lee, B. W. Kwon, M. Jung, D. Serhiichuk, D. Henkensmeier and Y. Kwon, *J. Power Sources*, **439**, 227079 (2019).
13. Y. Chung, C. Noh and Y. Kwon, *J. Power Sources*, **438**, 227063 (2019).
14. M. Skyllas-Kazacos, M. H. Chakrabarti, S. A. Hajimolana, F. S. Mjalli and M. Saleem, *J. Electrochem. Soc.*, **158**, R55 (2011).
15. C. Noh, S. Moon, Y. Chung and Y. Kwon, *J. Mater. Chem. A*, **5**, 21334 (2017).
16. C. Noh, C. S. Lee, W. S. Chi, Y. Chung, J. H. Kim and Y. Kwon, *J. Electrochem. Soc.*, **165**, A1388 (2018).
17. R. Chen, S. Kim and Z. Chang, *Redox Princ. Adv. Appl.*, 103 (2017).
18. M. Chen, P. Liu, Y. Li, Y. Hu, Z. Hu and Q. Wang, *J. Therm. Anal. Calorim.*, **147**, 4131 (2022).
19. T. N. Pham-Truong, Q. Wang, J. Ghilane and H. Randriamahazaka, *ChemSusChem*, **13**, 2142 (2020).
20. W. Lee, C. Jo, S. Youk, H. Y. Shin, J. Lee, Y. Chung and Y. Kwon, *Appl. Surf. Sci.*, **429**, 187 (2018).
21. M. Rychcik and M. Skyllas-Kazacos, *J. Power Sources*, **22**, 59 (1988).
22. I. Strużyńska-Piron, M. Jung, A. Maljusch, O. Conradi, S. Kim, J. H. Jang, H. J. Kim, Y. Kwon, S. W. Nam and D. Henkensmeier, *Eur. Polym. J.*, **96**, 383 (2017).
23. H. Y. Jung, M. S. Cho, T. Sadhasivam, J. Y. Kim, S. H. Roh and Y. Kwon, *Solid State Ionics*, **324**, 69 (2018).
24. C. Chu, B. W. Kwon, W. Lee and Y. Kwon, *Korean J. Chem. Eng.*, **36**, 1732 (2019).
25. W. Lee, G. Park, D. Chang and Y. Kwon, *Korean J. Chem. Eng.*, **37**, 2326 (2020).
26. W. Lee, A. Permatasari, B. W. Kwon and Y. Kwon, *Chem. Eng. J.*, **358**, 1438 (2019).
27. Y. Li, J. Sniekers, J. Malaquias, X. Li, S. Schaltin, L. Stappers, K. Binnemans, J. Fransaer and I. F. J. Vankelecom, *Electrochim. Acta*,



- 236, 116 (2017).
28. P. K. Leung, C. Ponce-De-León, C. T. J. Low, A. A. Shah and F. C. Walsh, *J. Power Sources*, **196**, 5174 (2011).
29. Y. Liu, M. A. Goulet, L. Tong, Y. Liu, Y. Ji, L. Wu, R. G. Gordon, M. J. Aziz, Z. Yang and T. Xu, *Chem*, **5**, 1861 (2019).
30. Y. Zhen, C. Zhang, J. Yuan, Y. Zhao and Y. Li, *J. Power Sources*, **480**, 229132 (2020).
31. B. Hu, J. Luo, M. Hu, B. Yuan and T. L. Liu, *Angew. Chemie*, **131**, 16782 (2019).
32. C. Noh, Y. Chung and Y. Kwon, *Chem. Eng. J.*, **405**, 126966 (2021).
33. C. Noh, Y. Chung and Y. Kwon, *J. Power Sources*, **466**, 228333 (2020).
34. S. E. Waters, B. H. Robb, M. P. Marshak and M. P. Marshak, *ACS Energy Lett.*, **5**, 1758 (2020).
35. M. Shin, C. Noh and Y. Kwon, *Int. J. Energy Res.*, **46**, 6866 (2022).
36. C. Noh, M. Shin and Y. Kwon, *J. Power Sources*, **520**, 230810 (2022).
37. M. Shin, C. Noh, Y. Chung and Y. Kwon, *Chem. Eng. J.*, **398**, 125631 (2020).
38. M. Shin, C. Noh, Y. Chung, D. H. Kim and Y. Kwon, *Appl. Surf. Sci.*, **550**, 148977 (2021).
39. C. Noh, B. W. Kwon, Y. Chung and Y. Kwon, *J. Power Sources*, **406**, 26 (2018).
40. Y. Chung, J. Jeong, H. T. T. Pham, J. Lee and Y. Kwon, *J. Electrochem. Soc.*, **165**, A2703 (2018).
41. B. Sun and M. Skyllas-Kazacos, *Electrochim. Acta*, **37**, 1253 (1992).
42. P. Mazúr, J. Mrlík, J. Beneš, J. Pocič, J. Vrána, J. Dundálek and J. Kosek, *J. Power Sources*, **380**, 105 (2018).
43. M. Jing, Z. Xu, D. Fang, X. Fan, J. Liu and C. Yan, *J. Electrochem. Soc.*, **168**, 030539 (2021).
44. Y. C. Chang, J. Y. Chen, D. M. Kabtamu, G. Y. Lin, N. Y. Hsu, Y. S. Chou, H. J. Wei and C. H. Wang, *J. Power Sources*, **364**, 1 (2017).
45. Y.-R. Dong, Y. Kawagoe, K. Itou, H. Kaku, K. Hanafusa, K. Moriuchi and T. Shigematsu, *ECS Trans.*, **75**, 27 (2017).
46. P. Mazur, J. Mrlík, J. Pocič, J. Vrána, J. Dundálek, J. Kosek and T. Bystron, *J. Power Sources*, **414**, 354 (2019).
47. M. Christwardana, Y. Chung and Y. Kwon, *Korean J. Chem. Eng.*, **34**, 3009 (2017).
48. K. Hyun, S. Kang and Y. Kwon, *Korean J. Chem. Eng.*, **36**, 500 (2019).
49. R. Wang, Y. Li and Y.-L. He, *J. Mater. Chem. A*, **7**, 10962 (2019).
50. H. R. Jiang, W. Shyy, M. C. Wu, R. H. Zhang and T. S. Zhao, *Appl. Energy*, **233-234**, 105 (2019).